Acta Cryst. (1986). A**42**, 484–492

Many-Beam Effects and Phase Information in Electron Channelling Patterns

BY KNUT MARTHINSEN AND RAGNVALD HØIER

Institutt for Røntgenteknikk, Universitetet i Trondheim-NTH, N-7034 Trondheim-NTH, Norway

(*Received* 20 *February* 1986; *accepted* 29 *April* 1986)

Abstract

Many-beam dynamical diffraction phenomena in channelling patterns using a scanning electron microscope have been studied in general with emphasis on effects due to non-systematic interactions in centrosymmetric crystals. As few beams as possible for a qualitative agreement between theory and experiment have been used, and the results are compared with effects observed using other diffraction techniques. The extensive intensity anomalies frequently observed near line intersections are explained through three-beam calculations. A channelling line is found to appear with enhanced or diminished contrast depending on the sign of the excitation error of the coupled beam and the value of the invariant phase sum of the three structure factors involved. The effects are easily identified in the patterns and are well suited for experimental determinations of phase invariants. This information may then profitably be utilized in structure studies in combination with results from other diffraction methods. Enhanced line segments from neighbouring intersections are found to combine to envelopes or inverted envelopes depending on the phase combination. The effects observed may be interpreted within two-beam terminology by means of effective structure factors and effective many-beam gap widths at the dispersion surface. Analytical expressions which illustrate this point are given.

Introduction

Selected area channelling patterns (SACP) may be observed in most scanning and transmission electron microscopes when the back-scattered electron intensity is registered as a function of the incident-beam direction. These patterns, which are a result of anomalous absorption effects in the specimen, were first discussed by Coates (1967), and the technique is at present well established experimentally (*e.g.* Booker & Humphreys, 1975). To interpret the observed effects several theoretical models have been suggested (Vicario, Pitaval & Fontaine, 1970; Reimer, Badde, Seidel & Bühring, 1971; Spencer, Humphreys & Hirsch, 1972; Yamamoto, Mori & Ishida, 1978; Spencer & Humphreys, 1980). So far these descriptions have adequately described the observed patterns on a qualitative or semi-quantitative level.

The channelling patterns have a wide range of uses especially in metallurgy and more recently also in geology. They may be utilized for lattice-parameter determination and in investigations of crystal orientation, texture and various types of deformations (*e.g.* Stickler, Hughes & Booker, 1971; Booker & Humphreys, 1975; Lloyd, Hall, Cockayne & Jones, 1981).

In addition to these applications the channelling patterns have a large potential for giving more detailed structure information. The possibilities are point-group and space-group determinations, and also determination of the invariant sum of the structure factor phases involved in three-beam interactions. Such applications have recently been investigated by Marthinsen (1986) and some preliminary results have been given by Marthinsen & Høier (1984).

As a rule all the diffraction effects utilized to obtain this structure information are dependent on a detailed understanding of non-systematic many-beam interactions, and such effects are hardly discussed in the literature for the channelling case. Only a brief comment has been given by Vicario, Pitaval & Fontaine (1970) while most papers concern effects due to systematic many-beam interactions (*e.g.* Booker & Humphreys, 1975; Farrow & Joy, 1980).

In another diffraction technique, *i.e.* the Kikuchi line case, the interpretation of non-systematic effects is well established (Kambe, 1957; Gjønnes & Høier, 1969, 1971; Høier, 1973). It is a question, however, whether these interpretations may be applied in the more complicated channelling case as well. To investigate this possibility and to increase the general use of channelling patterns in structure studies we have studied many-beam phenomena in channelling patterns in general with emphasis on the non-systematic diffraction effects. The present work concerns effects observed in centrosymmetric crystals. As experimentally determined three-phase invariants may profitably be utilized in combination with information from other structure determination methods, the dependence of three-beam diffraction effects on this invariant phase sum of the structure factors involved is especially investigated.

0108-7673/86/060484-09$01.50

Experimental

Selected area channelling patterns (SACP) have been obtained in a JSM-840 scanning electron microscope. A 40 kV diagram from Si is shown in Fig. 1 where the dominant lines belong to the [111] zone. Although such patterns resemble Kikuchi line patterns it should be noticed that their origin is different. They show the variation in the integrated electron back-scattering intensity as a function of the incident-beam direction, a variation which corresponds to the angular dependence of the anomalous absorption in the forward-scattered Bragg beams. Geometrically, however, the SACP look like Kikuchi patterns, and for this reason they have sometimes been termed pseudo-Kikuchi patterns.

A variety of intensity anomalies may be observed in the channelling patterns such as line segments with enhanced or diminished contrast near certain line intersections, kinematically forbidden lines, or very dark or bright regions near intersections between several low-index lines. A typical effect is seen at the intersection between the $\bar{3}\bar{1}5$ and $\bar{1}\bar{3}5$ lines in Fig. 1. A magnification of this intersection is reproduced in Fig. 2. Just inside the $\bar{1}\bar{3}5$ band, defined as the area between the $\bar{1}\bar{3}5$ line and the parallel $13\bar{5}$ line visible in the lower right-hand corner of Fig. 1, the $\bar{3}\bar{1}5$ line deviates in contrast and position from the simple two-beam prediction. The contrast is enhanced and the line is moved inwards compared with the ordinary two-beam position. Outside the $\bar{1}\bar{3}5$ band the $\bar{3}\bar{1}5$ line appears with almost vanishing contrast. The same description holds for the $\bar{1}\bar{3}5$ line, *i.e.* the $\bar{1}\bar{3}5$ line is diminished outside and enhanced inside the $\bar{3}\bar{1}5$ band. At the intersection the two enhanced segments combine to a curved line of hyperbolic shape. A similar effect is seen near the position on the $\bar{4}40$ line where the $\bar{5}15$ and $\bar{3}\bar{1}5$ lines intersect. The two lines split at the intersection point and the enhanced parts combine to a continuous segment. Enhanced segments inside the band of the coupled reflection are in fact observed at every intersection between the $(\bar{1}-2n, \bar{3}+2n, 5)$ lines, and the result is a smooth envelope. Several examples of such envelopes are seen in Fig. 1, where some of them are indicated by arrows.

A very special kind of envelope is the circle which for special voltages is clearly observed around the [111] zone axis. The line segments which constitute this circle result from incident beam directions where reciprocal-lattice points in the first-order Laue zone (FOLZ) below the equator layer fulfil the Bragg condition. The lines originating from the first upper layer are seen within the bright central area near the zone axis in Fig. 3. Similar types of FOLZ rings are frequently observed in convergent-beam patterns (Jones, Rackham & Steeds, 1977). The zone-axis channelling lines in Fig. 3 are the absorption analogue to the convergent-beam case when both direct-beam zone-axis lines and the corresponding FOLZ ring are observed.

For comparison with the non-systematic cases and to illustrate an additional diffraction effect a diagram showing the 111 systematic lines near the $[\bar{2}11]$ zone in Ge is included, Fig. 4. The lines forming the 111 band edges are hardly discernible. In accordance with previous observations in Si (Spencer, Humphreys &

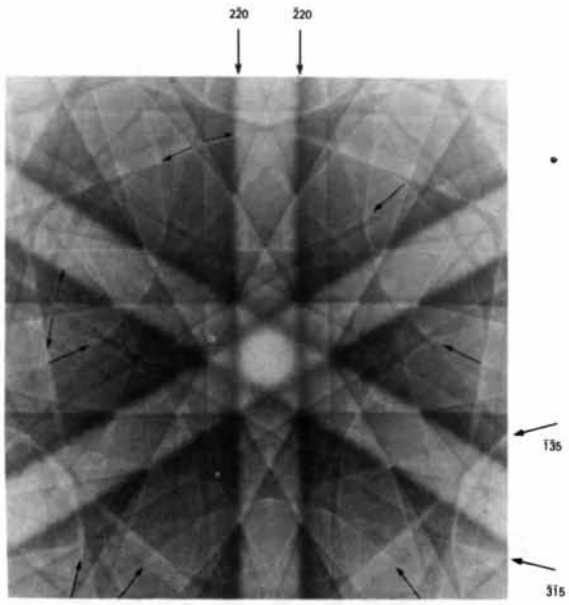

Fig. 1. SACP near the [111] zone in Si. 40 kV. Arrows show envelopes and FOLZ lines.

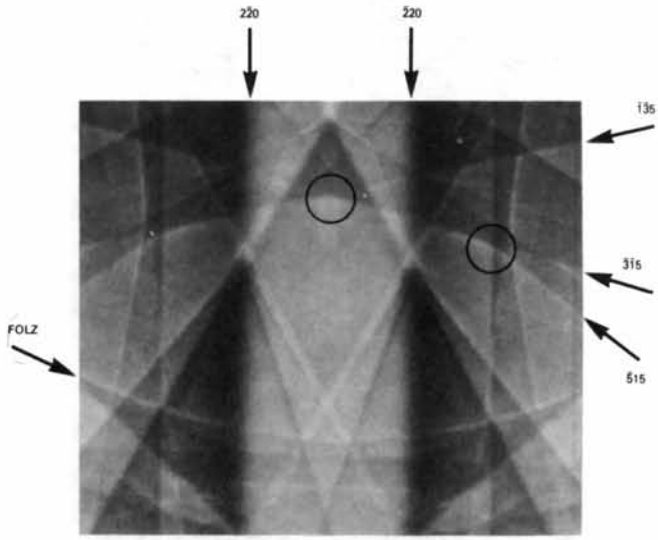

Fig. 2. Typical envelope in Si. 40 kV. Positions corresponding to calculations are encircled.

Hirsch, 1972) only a diffuse intensity maximum is seen. The 222 line contrast, however, is very strong although this reflection is forbidden in the diamond structure. In addition to the contrast anomalies at the ordinary line positions a dark line is observed in the middle of the 111 band. This line is extraordinary in the sense that it appears at a position which does not correspond to a two-beam Bragg condition.

Theory

Due to the complexity of the problem all the existing theoretical models necessarily have their weaknesses when applied to explain details in the observed patterns. But qualitatively, however, the agreement has so far been good. The calculations in the present work are based on the intensity expressions of Spencer, Humphreys & Hirsch (1972). From an interpretation point of view this description has been found to be the most suitable one although more complicated recent expressions are quantitatively better. If one concentrates on the many-beam diffraction aspects of the problem, this fact has been found to be of minor importance in the present studies.

To isolate the dominating intensity-determining parameters as few beams as possible have been used in the particular calculations reproduced below. For qualitative comparisons between theory and experiments three or four beams have proved to be sufficient in most cases.

The theory is based on a description of the fast electrons inside the crystal as a superposition of Bloch waves and each Bloch wave j is considered to back-scatter independently. The main mechanism responsible for the back scattering is assumed to be phonon scattering.

For a perfect crystal with thickness t the total back-scattered intensity, summed over all Bloch waves, is, at the crystal entrance surface ($z = 0$), given by

$$I_B(0) = (1 + p^0 t)^{-1}\{p^0 t + \sum_j I^j(0)[(p^j - p^0)/\mu^j] \times [1 - \exp(-\mu^j t)]\} \quad (1)$$

where μ^j is the intensity absorption coefficient for the jth Bloch wave. For near-normal incidence, $I^j(0) = |C_0^j|^2$. The back-scattering coefficients p^j are calculated from the phonon scattering theory of Hall & Hirsch (1965), *i.e.*

$$p^j = \frac{\pi}{\Omega N_c}\left[\frac{e^2 m Z \lambda^2}{4\pi\varepsilon_0 h^2}\right]^2 \sum_g \sum_h C_g^j C_h^{j*} \exp(-M_{h-g}) \times \sum_i \exp[i(\mathbf{h} - \mathbf{g}) \cdot \mathbf{r}_i] \quad (2)$$

and

$$p^0 = \sum_j p^j / n. \quad (3)$$

n is here the number of Bloch waves, Ω is the atomic volume, N_c is the number of atoms in the unit cell

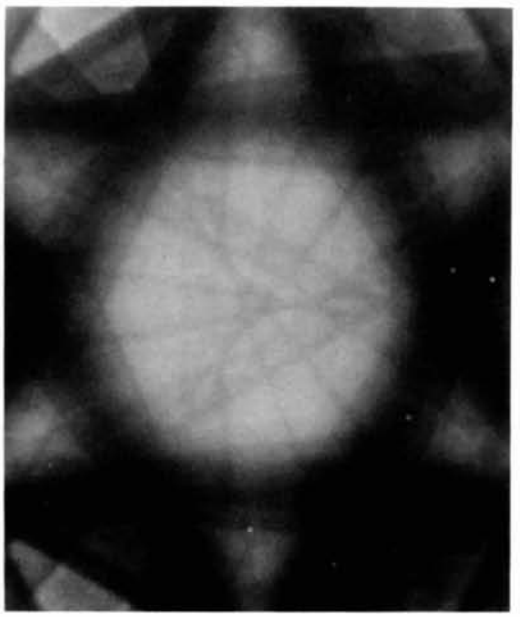

Fig. 3. Zone-axis FOLZ lines in Si. 22 kV.

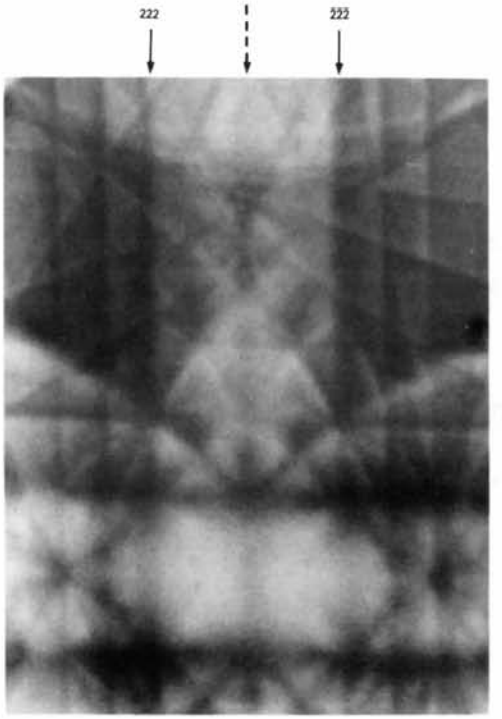

Fig. 4. 111 systematic lines in Ge showing line in the middle of the band. 40 kV.

and Z is the atomic number. $\mathbf{r}_i$ is the position of the ith atom in the unit cell while e, m and λ are the charge, mass and wavelength of the electron, respectively. h is Planck's constant, $\exp(-M_{h-g})$ is the Debye–Waller factor for the reflection $(\mathbf{h}-\mathbf{g})$ and C_g^j and C_h^j are components of the Bloch wave eigenvectors.

The eigenvectors and the corresponding *Anpassungen* γ^j defining the dispersion surface are found from the fundamental equation of standard many-beam electron diffraction theory (*e.g.* Humphreys, 1979). Further, the Bloch wave intensity absorption coefficients μ^j are calculated from the perturbation theory expression:

$$k\mu^j = U_0' + \sum_{g\neq h}\sum U'_{h-g} C_g^j C_h^{j*}. \qquad (4)$$

Here k is the wavevector and U'_{h-g} a Fourier coefficient of the imaginary part of the crystal potential. The real and imaginary parts of the potential have been taken from Radi (1970) and Doyle & Turner (1968).

The above intensity expression, however, is inadequate for bulk crystals, since $I_B(0)\to 1$ as $t\to\infty$. This problem is evaded theoretically by introducing a cut-off thickness t_b which represents the maximum depth to which an electron can penetrate before being back-scattered and re-emerging from the top surface of the crystal. We have chosen t_b to be $0{\cdot}4R_B$, where the Bethe range R_B is taken from Everhart & Hoff (1971).

A modified version of (1), which is based on (2) and thus valid only for simple monatomic structures, has been suggested by Schulson (1971). Generalizing to structures with different types of atoms, however, a position-dependent atomic number Z_i^2 and Debye–Waller factor should be included in the sum over i in (2). The result is a structure-factor-like term which typically may be taken to vary as U_{h-g} or U'_{h-g} with the reciprocal vectors. With the latter choice the double sum in (2) becomes equal to (4). Although it may be quantitatively inaccurate such an approximation is believed to take care of the typical variations in p^j with the diffraction condition. The following expression is obtained (a and b are positive constants and $\Delta\mu^j = \mu^j - \mu_0$):

$$I_B \sim a + b\sum_j |C_0^j|^2\,\Delta\mu^j. \qquad (5)$$

This equation couples in a simple way the back-scattering intensity to two well known factors, *i.e.* the Bloch wave excitation coefficients and the accompanying anomalous absorption parameters. Equation (5) is thus well suited for interpretational purposes. For the special case of two beams we obtain an expression which has the same angular variation as the equation given by Schulson (1971).

Calculations and discussion

The non-systematic three-beam case

The line patterns for the non-systematic cases to be discussed are the ones encircled in Fig. 2. A schematic diagram of the beam geometry and the lines of interest are shown in Figs. 5(a) and (b), respectively. In order to simulate the line pattern in the middle of the $2\bar{2}0$ band qualitatively, only the $\bar{1}\bar{3}5$ and $3\bar{1}5$ beams have to be taken into account. $T(x, y)$ in Fig. 5(a) is the projected centre of the Ewald sphere for this three-beam case where $x = y = 0$ when $\bar{1}\bar{3}5$ and $3\bar{1}5$ simultaneously fulfil the Bragg condition. The smaller circle in the figure is the intersection between the Ewald sphere and the reciprocal plane in this case.

The dynamical equations are solved for a set of diffraction conditions $T(x, y)$ near the common Bragg condition. For each diffraction condition the excitation errors, s_g, are found from the coordinates of the vector $\mathbf{T}$ from $x = y = 0$ to the point (x, y) and the reciprocal vectors of the different reflections, *viz*

$$ks_g = \mathbf{T}\,.\,\mathbf{g}. \qquad (6)$$

The calculated result for the intensity near the $3\bar{1}5$, $\bar{1}\bar{3}5$ line crossing is shown in Fig. 6(a), where a common background is subtracted. Qualitatively the calculations in Fig. 6(a) are in agreement with all the essential features in the observed line contrast in Fig. 2. The two lines involved appear both with enhanced contrast inside (lower hyperbola) and diminished contrast outside the band of the coupled reflection.

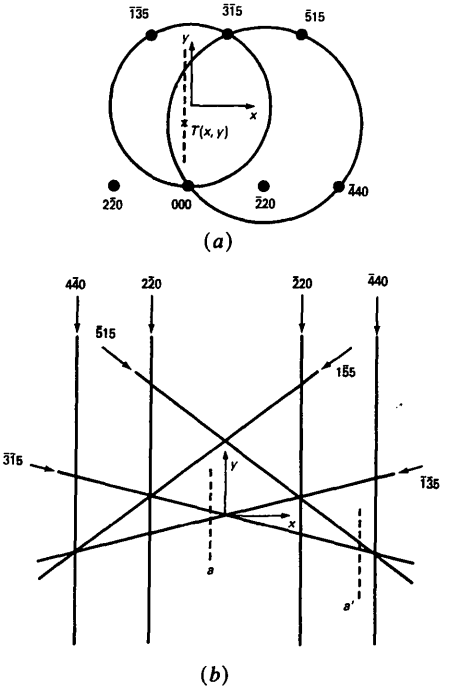

Fig. 5. (a) Beam geometry with projected centre of Ewald sphere, $T(x, y)$. (b) Lines referred to in calculations for Si.

They are further displaced from their ordinary two-beam positions near the line crossing, forming an enhanced curved segment. This line displacement is asymptotically approaching the two-beam position with increasing distance from the line crossover in accordance with the observations in Fig. 2. To interpret these contrast changes, section a in Fig. 6(a), corresponding to $T(a, y)$, $a<0$, in Fig. 5, has been selected for more detailed investigations. The dispersion surface and the corresponding variation in the excitation coefficients are shown in Figs. 7(a) and (b) where the deviation parameter, y, and the excitation error, s_g, are negative inside the band, *i.e.* in the lower part of Fig. 6. In Fig. 7(a) the dashed lines indicate the spheres around the reciprocal points, and the vertical heavy lines show by their position and length the two-beam position and gap width, respectively.

The three-beam gaps in Fig. 7(a) are displaced in opposite directions resulting in a larger intergap distance. Further, the gap at $y<0$ ($\bar{1}\bar{3}5$ line) is enhanced and the other one ($\bar{3}\bar{1}5$ line) diminished with respect to the two-beam value. These differences are reflected in the excitation coefficients, Fig. 7(b). As expected, the branch nearest to the O sphere is the most strongly excited one, and it should be noticed that the position where the strong excitation changes from one branch to another is always associated with the many-beam gap position. Further, the width of the area where large changes in branch excitation take place is largest near the largest gap. The variations in $|C_0^j|^2$ shown in Fig. 7(b) are typical for all the examples discussed below as well.

The calculated variations in p^j and μ^j with y are reproduced in Figs. 8(a) and (b). As expected from the discussion above, p^j and μ^j are seen to have a similar type of variation with the diffraction condition, and the relative variation in μ^j is generally found to be small compared with the relative variation in p^j. This similarity in the variations of p^j and μ^j is found to be typical for the cases studied in the present work.

The profile a in Fig. 6 may now be fully understood from (5) [or (1)]. Inside the $\bar{1}\bar{3}5$ band the line contrast is dominated by the branch-1 contribution as both $|C_0^1|^2$ and $\Delta\mu^1$ (or Δp^1) are simultaneously non-negligible and positive. The intensity increases to a maximum essentially due to the increase in $\Delta\mu^1$ with decreasing distance from the gap. If y is increased further the branch-2 contribution takes over, giving

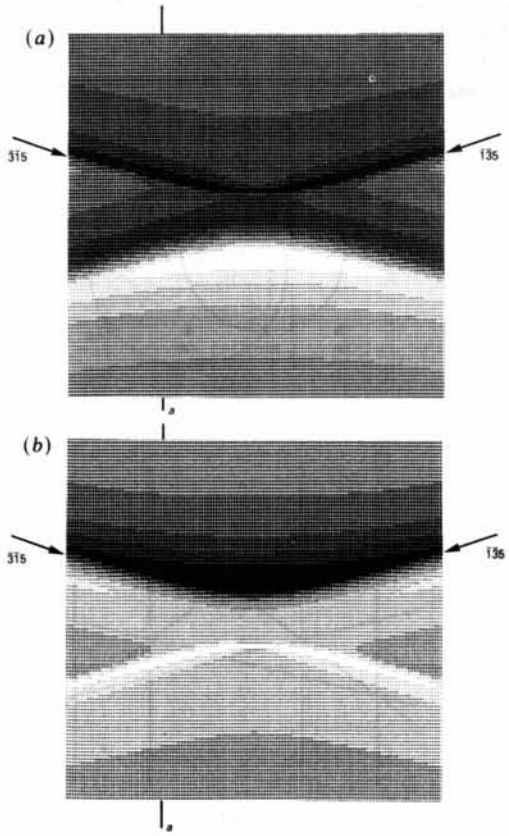

Fig. 6. Calculated $\bar{3}\bar{1}5$, $\bar{1}\bar{3}5$ three-beam contrast. (a) $\psi=0$, (b) $\psi=\pi$.

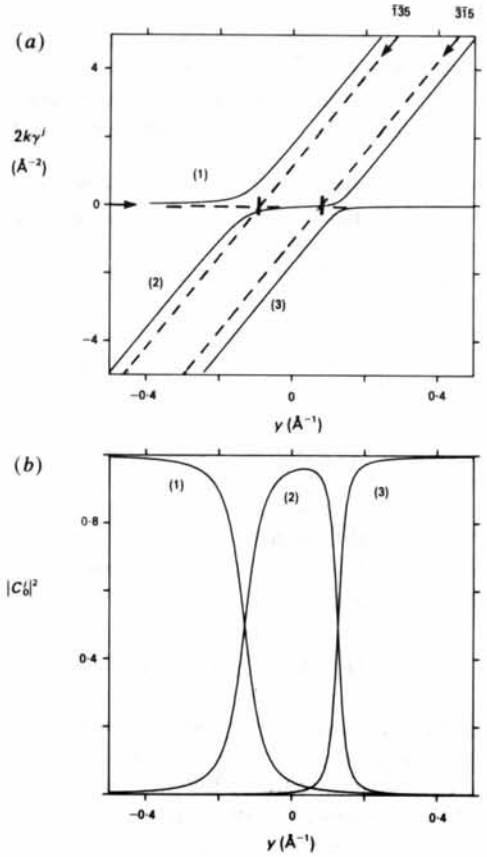

Fig. 7. $\bar{3}\bar{1}5$, $\bar{1}\bar{3}5$ three-beam case, section a. $\psi=0$. (a) Calculated dispersion surface as function of the deviation parameter y. (b) Calculated excitation coefficients.

a contrast which first decreases and then increases again towards the $\bar{3}\bar{1}5$ gap. This variation follows the $\Delta\mu^2$ (or Δp^2) variation. Close to the $\bar{3}\bar{1}5$ gap a similar change takes place with increasing y now between the branches 2 and 3. Here, however, the gap is smaller and all the effects are thus less pronounced. This discussion thus clearly demonstrates that the effects observed may profitably be associated with the dispersion surface gaps which both through their position and width determine the line position and contrast. It should also be noted that the gap and the contrast in this case are diminished when the excitation error of the coupled reflection is positive.

A hypothetical three-beam case

As for all three-beam cases in Si the product between the Fourier potentials involved is positive, *i.e.*

$$P = U_{-h}U_gU_{h-g} > 0. \tag{7}$$

After introduction of the phases φ_g of U_g *etc.* the corresponding three-phase invariant

$$\psi = \varphi_{-h} + \varphi_g + \varphi_{h-g} \tag{8}$$

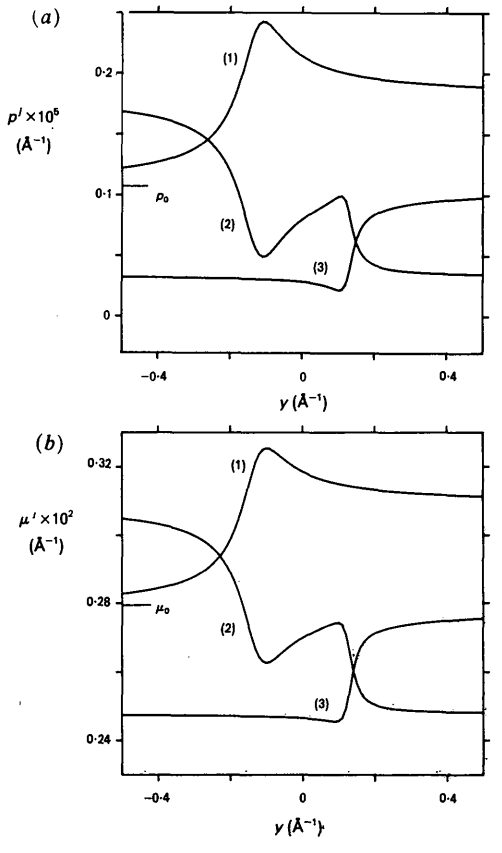

Fig. 8. $\bar{3}\bar{1}5$, $\bar{1}35$ three-beam case, section a. $\psi = 0$. (a) Calculated back-scattering coefficients. (b) Calculated absorption parameters.

is always zero for Si. But as an example of another centrosymmetric case the product P may hypothetically be taken to be negative through a sign shift in one of the Fourier potentials. The calculated line contrast for $\psi = \pi$ or $P < 0$ is shown in Fig. 6(b). When compared with Fig. 6(a) clear differences are observed. The two lines now appear with diminished contrast inside and enhanced contrast outside the band of the coupled reflection, and the enhanced line segments again combine to form an enhanced curved line, but in this case outside the band. A cut through the dispersion surface at a in Fig. 6(b) is presented in Fig. 9. This section corresponds to section a in Fig. 6(a). The $\bar{1}35$ line is in this case associated with the smaller gap. The contrast follows from the narrow angular variation of the excitation coefficients and the corresponding small relative variations in the back-scattering coefficients. On the other hand, the enhanced $\bar{3}\bar{1}5$ line contrast outside the band may be ascribed to the width of the larger gap at this position.

The channelling envelope

The calculations above clearly demonstrate the origin of the $(\bar{1}-2n, \bar{3}+2n, 5)$ and similar types of envelopes in Fig. 1. They may basically be ascribed to the three-beam effects near each intersection and result when the enhanced segments at neighbouring intersections combine to form a smooth curve. The ordinary channelling envelopes therefore only appear when $\psi = 0$ ($P > 0$). When $\psi = \pi$ ($P < 0$) the line segments outside the bands are enhanced, resulting in a wave-like figure which could be termed an inverted channelling envelope.

Similar types of envelopes are well known in Kikuchi patterns. In a simple model the envelopes observed from relatively thin crystals may here be ascribed to factors of the type $|C_0^j|^4$ (deficient) and $|C_0^j C_h^j|^2$ (excess). Like the factors in (5) both of these have angular half widths which follow the dispersion-surface gap width. This is the reason why the variations in the contrast with the angular deviation parameters are so similar in the Kikuchi and channelling many-beam cases.

Comparison may be even more interesting with Kikuchi patterns from thick crystals. Here the Kikuchi band contrast is typically given by $|C_0^j|^2 \exp(-\mu^j t)$ (*e.g.* Høier, 1973). Comparison with (5) therefore illustrates the complementarity between the two methods. At the band edge the large $\Delta\mu^1$ of the Bloch wave 1 results in a large exponential absorption term and a minimum intensity inside the Kikuchi band. Immediately outside the band the negative $\Delta\mu^2$ leads to a maximum. (5) gives the opposite variation. This complementarity is also expected intuitively, *i.e.* when the forward transmission is high the back-scattering is low and *vice versa*.

Contrast determining parameters

The essential parameters for the contrast in one line, h, are the value of the three-phase invariant ψ (or the product P) and the excitation error of the simultaneously excited beam, s_g, *i.e.* $I_B^h(\psi, s_g)$. Dependences of the diffracted intensity on these parameters have also been discussed in transmission electron diffraction (*e.g.* Shinohara, 1932; Kambe, 1957; Gjønnes & Høier, 1969, 1971) and in the X-ray case (*e.g.* Post, 1979; Høier & Marthinsen, 1983; Chang, 1984; Juretschke, 1984). It has in particular been shown for the three-beam case (Gjønnes & Høier, 1971) that a zero gap width may generally be found with centrosymmetric crystals for the following excitation errors ($\psi = 0$ or π):

$$2ks_g = \frac{|U_g|(|U_{g-h}|^2 - |U_h|^2)}{|U_h||U_{g-h}|\cos\psi}$$
$$2ks_h = \frac{|U_h|(|U_{g-h}|^2 - |U_g|^2)}{|U_g||U_{g-h}|\cos\psi}. \qquad (9)$$

These equations determine the position of zero gap and may hence be utilized in the channelling case to locate the position of minimum or zero line contrast. From Fig. 6 the coupling U_{g-h} is a factor of five larger than U_h. U_h and U_g are equal and $\psi = 0$ in Fig. 6(a) and $\psi = \pi$ in Fig. 6(b). The position of the zero gap width is obtained from (9) which gives $s_g = s_h$. This corresponds to the central point of the diminished hyperbola in Fig. 6 where the contrast is seen to be very low. A similar effect may be seen on the low-contrast hyperbola in Fig. 10(b). $U_{\bar{5}15}$ is the smallest factor in this case and the zero contrast position on this line is found outside the $\bar{3}\bar{1}5$ band when $\psi = 0$ and inside when $\psi = \pi$ in accordance with (9).

As is evident from Fig. 1 a very large number of three-beam interactions may easily be observed in a single print. A very large number of phase invariants may hence unambiguously be determined experimentally. In view of the standard phase problem in diffraction experiments such a starting set of known phase sums should be of great value when combined with results from other structure determination methods.

It also seems clear that the enhanced and diminished line contrast may profitably be interpreted in terms of an effective gap width determined by an effective Fourier coefficient, U_h^{eff}, being smaller or larger than the corresponding two-beam value. Such effective values may be found in many-beam solvable cases or by use of approximation methods like the second Bethe approximation. Utilizing the latter

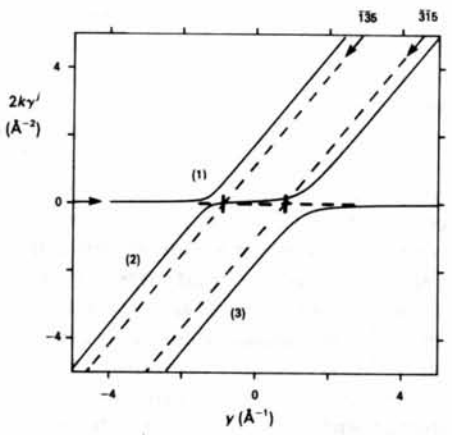

Fig. 9. Calculated dispersion surface for the $\bar{3}\bar{1}5$, $\bar{1}\bar{3}5$ three-beam case, section a. $\psi = \pi$.

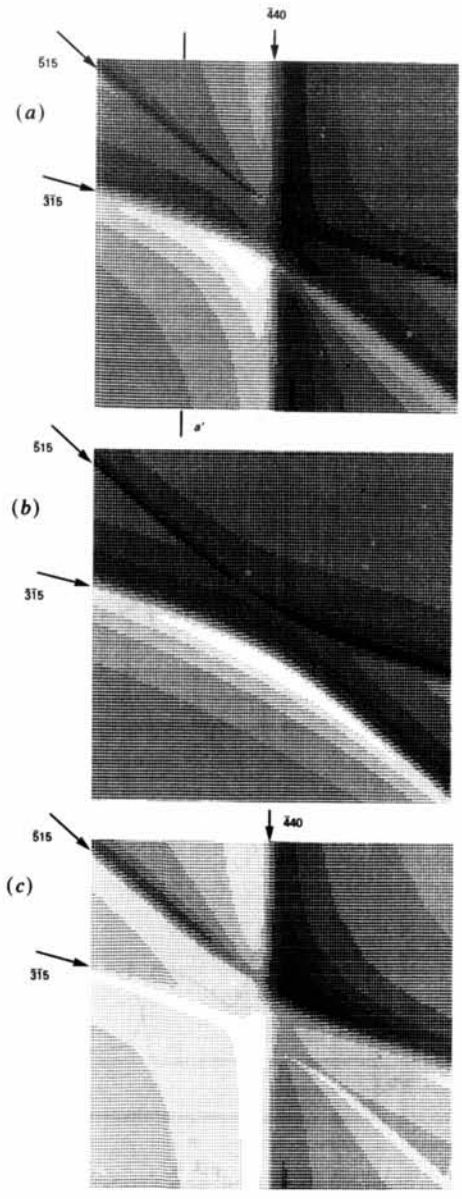

Fig. 10. Calculated contrast. (a) Four beams. $\psi = 0$ for dominating interaction. (b) Three beams. $\psi = 0$. (c) Four beams. $\psi = \pi$.

approach the following solution for U_h^{eff} in centrosymmetric crystals is found:

$$U_h^{\text{eff}} = U_h\left[1-\frac{|U_g||U_{h-g}|}{|U_h|2ks_g}\cos(\varphi_{-h}+\varphi_g+\varphi_{h-g})\right]. \quad (10)$$

When $\psi=0$, U_h^{eff} is therefore smaller than U_h outside the band of the coupled reflection, *i.e.* when $s_g>0$, in accord with the exact solution (9). In addition (10) shows that the effects are strongest in the weakest beam, and that the effect increases with increasing Fourier coefficients of the coupled and the coupling reflections.

A four-beam non-systematic case

The beam geometry of the four-beam case, *i.e.* 000, $\bar{3}\bar{1}5$, $\bar{5}15$, $\bar{4}40$, corresponds to the larger circle in the schematic drawing in Fig. 5. The calculated line contrast is shown in Fig. 10(*a*). A comparison with the observed line contrast in Fig. 2 shows good agreement with respect to all the essential features in this figure. A section a' through the dispersion surface [see Fig. 5 and Fig. 10(*a*)] parallel to the $\bar{4}40$ line position is shown in Fig. 11. The angular variation of p^j and the dependence on the gap width is in principle the same in this case as with three beams. The $\bar{3}\bar{1}5$ and $\bar{5}15$ line contrast are coupled to the two gaps positioned near the intersection between the spheres around the reciprocal-lattice points $\bar{3}\bar{1}5$ and $\bar{5}15$ and the O sphere, *i.e.* the two upper gaps in Fig. 11. In addition to the displacement from their two-beam position, which is responsible for the splitting of the two lines, the gaps deviate strongly from the two-beam values resulting in an enhanced $\bar{3}\bar{1}5$ contrast and a diminished $\bar{5}15$ contrast for these diffraction conditions.

The main contrast variations in this four-beam interaction are governed by the $\bar{3}\bar{1}5$, $\bar{5}15$ three-beam interaction for diffraction conditions not too close to the four-beam condition. This is seen from Fig. 10(*b*)

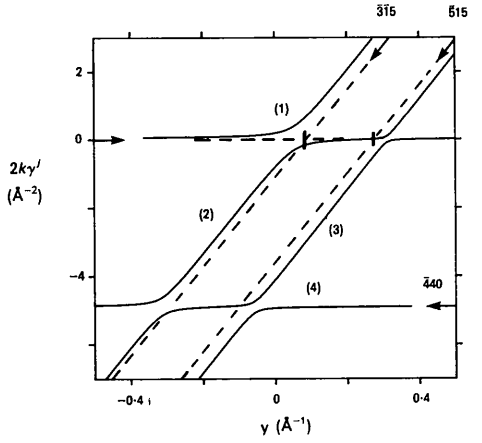

Fig. 11. Calculated dispersion surface for $\bar{3}\bar{1}5$, $\bar{5}15$, $\bar{4}40$ four-beam case, section a'. $\psi=0$ for dominating interaction.

where a three-beam calculation has been performed for the same diffraction conditions as in Fig. 10(*a*), but $\bar{4}40$ is now omitted. The enhanced segments combine to form a part of the ordinary envelope constituted by the $(\bar{1}-2n, \bar{3}+2n, 5)$ lines ($\psi=0$).

The effect of theoretically reversing the sign of the product between the Fourier potentials involved, *i.e.* putting $\psi=\pi$, is similar to that observed in Fig. 6. The line segments corresponding to the ordinary envelope are reduced in contrast and strongly enhanced segments will appear outside the band of the coupled reflection. Except for very close to the four-beam condition these variations are not affected by taking $\bar{4}40$ into account, as is shown in Fig. 10(*c*).

The reason why the four-beam case is dominated by the particular three-beam interaction discussed is due to the relative values of the Fourier coefficients involved. Since we have found that the contrast anomalies in the different lines can be understood from an effective dispersion surface gap width, the conclusions from above may be applied in this case as well. The effects are most pronounced in a weak reflection, when strongly coupled to another not too weak reflection as shown by (10). At least the first condition, a strong coupling reflection, is fulfilled for the 000, $\bar{3}\bar{1}5$, $\bar{5}15$ three-beam case where the coupling is $U_{\bar{2}\bar{2}0}$. The $\bar{5}15$ line contrast is strongly influenced both in position and amount by the $\bar{3}\bar{1}5$ reflection *via* the coupling $\bar{2}\bar{2}0$ and *vice versa*. The $\bar{4}40$ line, however, is weakly coupled to the other reflections involved, thereby explaining the negligible influence of this reflection on the contrast. The same explanations apply at every intersection between two of the $(\bar{1}-2n, \bar{3}+2n, 5)$ lines, a three-beam interaction dominates and $\bar{2}\bar{2}0$ is responsible for the coupling. Since all the three-beam cases in Si have $\psi=0$ ($P>0$) a pronounced envelope is thus formed inside these lines.

Inclusion of more than three or four beams in the above calculations will only cause minor differences in the calculated contrast, not altering the essential features of the many-beam effects.

A systematic many-beam case

The calculated intensity half-profile for the 111 systematic lines in Ge is shown in Fig. 12(*a*) (11 beams). Comparing Fig. 12(*a*) with Fig. 4 we see that the calculated line contrast is qualitatively in agreement with the observed contrast details. The 111 band edge appears with quite indistinct contrast, while the kinematically forbidden second-order line is well defined and relatively strong. In addition a clear minimum in back-scattered intensity is found at the symmetry position.

The very weak 111 line contrast may be understood from the branch-1 and -2 contributions in Fig. 12. While $\Delta\mu^1$ (Δp^1) is found to be approximately constant in this case, $\Delta\mu^2$ (Δp^2) varies more strongly with

the diffraction condition. This variation in the two important back-scattering coefficients combined with the slow interchange between the branch-1 and -2 excitations accounts for the slowly varying intensity changes near the 111 line position. In fact this is consistent with two-beam considerations (5). The maximum intensity inside the line position may, according to such expressions, appear close to the middle of the band, thus smearing out the contrast of the band edge. Two-beam considerations cannot, of course, be applied to the back-scattered intensity minimum observed at the band centre which does not correspond to an ordinary line position. This minimum in Fig. 12 corresponds to the enhanced branch-3 contribution at the symmetry position which may be observed in standard transmission experiments (*e.g.* Humphreys, 1979). The minimum is associated with the dispersion surface gap between branch 2 and 3 and may be ascribed to the branch-3 contribution. From Fig. 12(*b*) it is seen that, in addition to branch 1, branch 3 is quite strongly excited at the band centre and the pronounced minimum in branch-3 absorption parameter at this position causes the minimum in I_B.

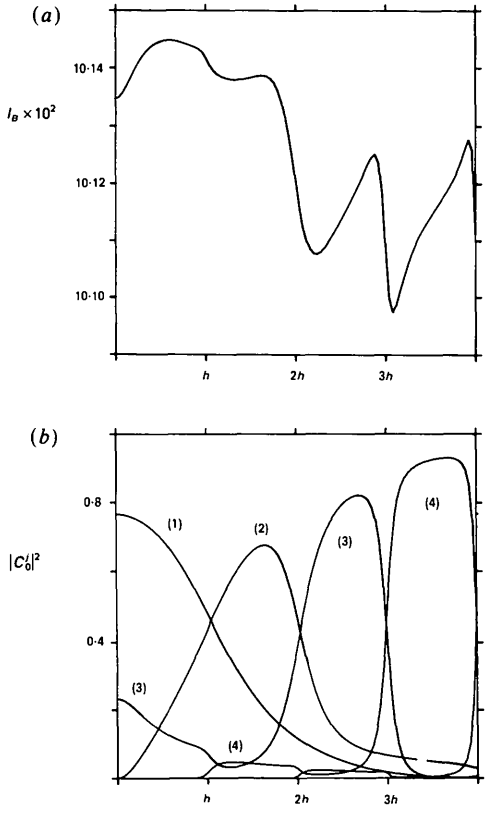

Fig. 12. 111 band in Ge. (*a*) Calculated contrast. (*b*) Calculated excitation coefficients. 11 beams.

The 222 line contrast, which from two-beam considerations should be zero, can be ascribed to the many-beam second-order gap. The contrast is due to the difference in the back-scattering coefficients of Bloch waves 2 and 3 which are the ones primarily excited for this orientation. The appearance of this line may also be explained from the Bethe approximation which gives a main term in the second-order gap width equal to $|U_{111}|^2/k|s_{111}|$.

As in the non-systematic case, the contrast variations are therefore always found to be associated with the widths and the positions of the gaps at the dispersion surface. The gap displacement is, however, small in the systematic case.

References

BOOKER, G. R. & HUMPHREYS, C. J. (1975). *Electron Microscopy in Material Science*, edited by U. VALDRÈ & R. RUEDL, Vol. IV, pp. 1199-1248. Luxembourg: Commission of the European Communities.

CHANG, S. L. (1984). *Multiple Diffraction of X-rays in Crystals.* Berlin: Springer.

COATES, D. G. (1967). *Philos. Mag.* **16**, 1179-1184.

DOYLE, P. A. & TURNER, P. S. (1968). *Acta Cryst.* A**24**, 390-397.

EVERHART, T. E. & HOFF, P. H. (1971). *J. Appl. Phys.* **42**, 5837-5846.

FARROW, R. C. & JOY, D. C. (1980). *Phys. Rev. Lett.* **44**, 1590-1593.

GJØNNES, J. & HØIER, R. (1969). *Acta Cryst.* A**25**, 595-602.

GJØNNES, J. & HØIER, R. (1971). *Acta Cryst.* A**27**, 313-316.

HALL, C. R. & HIRSCH, P. B. (1965). *Proc. R. Soc. London Ser. A*, **286**, 158-177.

HØIER, R. (1973). *Acta Cryst.* A**29**, 663-672.

HØIER, R. & MARTHINSEN, K. (1983). *Acta Cryst.* A**39**, 854-860.

HUMPHREYS, C. J. (1979). *Rep. Prog. Phys.* **42**, 1825-1887.

JONES, P. M., RACKHAM, G. M. & STEEDS, J. W. (1977). *Proc. R. Soc. London Ser. A*, **354**, 197-222.

JURETSCHKE, M. J. (1984). *Acta Cryst.* A**40**, 379-389.

KAMBE, K. (1957). *J. Phys. Soc. Jpn*, **12**, 13-25.

LLOYD, G. E., HALL, M. G., COCKAYNE, B. & JONES, D. W. (1981). *Can. Mineral.* **19**, 505-518.

MARTHINSEN, K. (1986). In preparation.

MARTHINSEN, K. & HØIER, R. (1984). *Acta Cryst.* A**40**, C384.

POST, B. (1979). *Acta Cryst.* A**35**, 17-21.

RADI, G. (1970). *Acta Cryst.* A**26**, 41-56.

REIMER, L., BADDE, H. G., SEIDEL, H. & BÜHRING, W. (1971). *Z. Angew. Phys.* **31**, 145-151.

SCHULSON, E. M. (1971). *Phys. Status Solidi B*, **46**, 95-101.

SHINOHARA, K. (1932). *Sci. Pap. Inst. Phys. Chem. Res. Jpn*, **20**, 39-51.

SPENCER, J. P. & HUMPHREYS, C. J. (1980). *Philos. Mag.* A**42**, 433-451.

SPENCER, J. P., HUMPHREYS, C. J. & HIRSCH, P. B. (1972). *Philos. Mag.* **26**, 193-213.

STICKLER, R., HUGHES, C. W. & BOOKER, G. R. (1971). Proc. Seventh Ann. Scanning Electron Microscopy Symp. Vol. I, pp. 473-483.

VICARIO, E., PITAVAL, M. & FONTAINE, G. (1970). *Proc. Seventh International Congress on Electron Microscopy, Grenoble*, Vol. 2, pp. 211-212. Paris: Société Francaise de Microscopie Electronique.

YAMAMOTO, T., MORI, M. & ISHIDA, Y. (1978). *Philos. Mag.* A**38**, 439-461.